Available online at www.sciencedirect.com

ScienceDirect

Geochimica et Cosmochimica Acta 124 (2014) 272–282

Geochimica et Cosmochimica Acta

www.elsevier.com/locate/gca

Coupled effects of temperature and mass transport on the isotope fractionation of zinc during electroplating

Jay R. Black [a,1], Seth G. John [b,2], Abby Kavner [a,*]

[a] Department of Earth, Planetary, and Space Sciences, University of California, Los Angeles, CA 90095, United States
[b] Division of Geological and Planetary Sciences, California Institute of Technology, Pasadena, CA 91125, United States

Received 18 March 2013; accepted in revised form 14 September 2013; available online 27 September 2013

Abstract

The isotopic composition of zinc metal electrodeposited on a rotating disc electrode from a Zn-citrate aqueous solution was investigated as a function of overpotential (electrochemical driving force), temperature, and rotation rate. Zn metal was measured to be isotopically light with respect to Zn^{+2} in solution, with observed fractionations varying from $\Delta^{66/64}Zn_{metal\text{-}aqueous} = -1.0‰$ to $-3.9‰$. Fractionation varies continuously as a function of a dimensionless parameter described by the ratio of observed deposition rate to calculated mass-transport limiting rate, where larger fractionations are observed at lower deposition rates, lower temperature, and at faster electrode rotation rates. Thus, the large fractionation and its rate dependence is interpreted as a competition between the two kinetic processes with different effective activation energies: mass-transport-limited (diffusion limited) kinetics with a large activation energy, which creates small fractionations close to the predicted diffusive fractionation; and electrochemical deposition kinetics, with a smaller effective activation energy, which creates large fractionations at low deposition rates and high hydrodynamic fluxes of solute to the electrode. The results provide a framework for predicting isotope fractionation in processes controlled by two competing reactions with different kinetic isotope effects.

1. INTRODUCTION

Zinc is a relatively abundant transition metal on the surface of the Earth, and its isotopic behavior is a marker for a variety of different processes in geology, biology, and industry (for a review see Cloquet et al., 2008), including genesis and chemical weathering of hydrothermal ore deposits (e.g. Fernandez and Borrock, 2009; Fujii et al., 2011; Gagnevin et al., 2012), volcanic processes (e.g. Toutain et al., 2008), biological uptake in plants from local groundwater and soils (e.g. Weiss et al., 2005; Moynier et al., 2009; Arnold et al., 2010; Jouvin et al., 2012); and quantification of anthropogenic fluxes into the environment (Borrok et al., 2009; Chen et al., 2009; Mattielli et al., 2009; Bigalke et al., 2010; Juillot et al., 2011; Fujii and Albarede, 2012). The use of metal stable isotopes as process tracers in relevant environments requires that the mechanism(s) for isotope fractionation must be understood and quantified. For natural systems, the amount of fractionation expressed during chemical reaction often depends both on the inherent isotope effect for the reaction, and mass-transport limitation. Under mass-transport limited conditions, the chemical reaction takes place more quickly than the reactant can be replaced, leading to a change in the isotopic composition of the reactants which, in turn, typically leads to a decrease in the magnitude of the expressed isotope effect compared to the maximum isotope effect that would be expressed in non-mass transport limited conditions.

* Corresponding author. Tel.: +1 310 206 3675.
E-mail addresses: jayrblack@gmail.com (J.R. Black), sjohn@geol.sc.edu (S.G. John), akavner@ucla.edu (A. Kavner).
[1] Present address: Peter Cook Centre for CCS Research, School of Earth Sciences, The University of Melbourne, Melbourne, VIC 3010, Australia. Tel.: +61 3 90355218.
[2] Present address: Department of Earth and Ocean Sciences, University of South Carolina, Columbia, SC 29208, United States. Tel.: (803) 777-7052.

0016-7037/$ - see front matter © 2013 Elsevier Ltd. All rights reserved.
http://dx.doi.org/10.1016/j.gca.2013.09.016

While Zn(II) is the only stable redox state for Zn in natural evironments, many of the largest observed single-pass isotope separations (i.e. those which are due to a single chemical process, as opposed to reservoir evolution and/or multi-stage cascade processes) are observed in systems containing one or more redox states. We have therefore performed a series of laboratory electrochemistry experiments consisting of electroplating metal from an aqueous metal-salt reservoir, which allows us to simultaneously explore isotopic fractionation associated with redox processes, and to observe how such fractionations are tempered by mass-transport limitation. Laboratory electrochemistry provides a way to examine rate-dependent isotope fractionations while simultaneously controlling other variables relevant to kinetic processes such as temperature, species concentration, and mass transport to the reacting surface. These experiments have been performed under a variety of different conditions and different metals, including iron (Kavner et al., 2005, 2009; Black et al., 2010a,b), zinc (Kavner et al., 2008; Black et al., 2010a), copper (Black et al., 2011a) and lithium (Black et al., 2009). For all of these systems, the isotope fractionation factors between the electroplated metal and the stock solution show similar and sometimes surprising trends. Below we summarize our previous observations and their preliminary interpretations:

- *Light isotopes are electroplated.* In all cases light stable isotopes of the metals are preferentially electroplated, with mass-dependent behavior evident where three or more isotopes are measured.
- *Fractionation is time-independent, meaning that the fractionation factor does not vary with the extent of reaction.* In most of our experiments, we have controlled the extent of reaction such that only a small amount of metal is deposited from the stock solution, thus avoiding significant evolution of the reservoir composition. In such experiments, the observed isotope fractionation is constant as a function of time (amount electroplated), as long as the electroplating rate and other factors are held constant. In the one case where we continuously electroplated zinc while monitoring the isotopic evolution of the plated material and the remaining stock solution (Kavner et al., 2008), the data could be fit within error by assuming a Rayleigh distillation of the reservoir and using a constant isotope fractionation factor equal to the isotope effect observed at low extents of reaction.
- *Fractionation does not depend on electrode composition.* In the cases where experiments were performed on different electrode compostions (i.e. gold vs. platinum vs. glassy carbon) but with otherwise identical variables, observed isotope signature of the plated material remains unchanged.
- *Fractionation increases as temperature increases.* Planar electrode deposition experiments as a function of temperature showed larger fractionations at higher temperatures.
- *Fractionation is dependent on rate/overpotential.* Generally, the observed fractionation decreases monotonically as the overpotential is increased, and increases as the stir rate of the plating solution is increased. In the experiments where a rotating disc electrode is used to control the supply of solution to the electrode, larger rotation rates generate larger fractionations.
- *Maximum observed fractionations are generally higher than predicted equilibrium fractionations.* Our observed fractionation factors vary depending on experimental conditions as listed above, but the fractionation factors that arise from the slowest kinetic conditions are the largest, larger than the predicted equilibrium fractionation factors for all elements, with the exception of Li where the maximum fractionation is approximately equal to the predicted equilibrium value (Black et al., 2009).

Taken together, this set of observations suggests that at least two competing processes determine the overall observed isotope fractionation of metals during electroplating. In Black et al. (2010a) a competition between mass-transport and electrochemical kinetics is invoked to explain the observed fractionation that increases with temperature.

Our goal in this paper is to test the hypothesis raised in our previous papers by performing a series of electroplating experiments in which the reaction over-potential, temperature, and mass transport to the electrode are all independently-controlled. Measured isotope fractionation can then be compared directly with results of a quantitative model predicting isotope behavior when mass-transport kinetics and electrochemical deposition kinetics are competing. Zinc is an ideal metal for these experiments. In most natural systems, zinc exists as Zn(II) either in aqueous solution or in an oxide or sulfide mineral. Therefore, while our study on electrodeposition of ZnII to Zn metal does not have direct application in terms of interpreting Zn isotope signatures in the environment, the goal of this study is to use Zn electrodeposition as a model system to examine isotope fractionation during processes which involve competition from two or more kinetic steps. Previous experience has shown us that Zn electroplating kinetics is well behaved in practice; isotope fractionations tend to have high repeatability, and the observed fractionations are large. In fact, Zn has the largest observed single pass fractionation when normalized to the percent mass difference between isotopes. Experimentally we find that the plating efficiencies for zinc are high; therefore we assume that competing reactions at the electrode are minimized. In addition, our recent work examines Zn(II) ion speciation as a function of solution chemistry as well as using *ab initio* methods to calculate the partition function ratios of various aqueous zinc isotopologue species (Black et al., 2011b). The theoretical predictions (Black et al., 2011b) can be tested by studying temperature-dependent fractionation as a function of mass transport to a rotating disc electrode.

2. EXPERIMENTAL METHODS

2.1. Electroplating experiments

In all experiments, a small (<0.2% of starting solution) amount of zinc metal was electroplated onto a rotating disc electrode from aqueous plating solutions under constant

voltage and temperature conditions. The resulting plated samples were collected and their isotope composition with respect to the starting solution was measured using high resolution MC-ICP-MS. For all of these zinc electrodeposition experiments, a stock solution consisting of 0.1 molal zinc buffered by 0.52 molal citrate was prepared from $ZnSO_4 \cdot 7H_2O$ and $Na_3C_6H_5O_7 \cdot 2H_2O$ salts and its pH adjusted with H_2SO_4 to a final pH of 3.8 (buffered between pKa2 and pKa3 for citrate). See Table S2 (Supplementary material)for final stock solution composition and speciation calculations (Black et al., 2011b). We chose zinc citrate so that we could better buffer the stock solutions at a constant pH, unlike in our previous experiments using Zn sulfate (Kavner et al., 2008; Black et al., 2010a), and Zn chloride (Black et al., 2010a). In addition, we have performed calculations of temperature-dependent equilibrium isotope fractionation between Zn^{II}citrate and Zn metal (Black et al., 2011b).

Electroplating experiments were performed using an Autolab potentiostat (PGSTAT30) using a 3 mm diameter platinum rotating disc electrode (RDE) whose rotation rate can be varied, thus controlling mass transport by hydrodynamic supply of solution to the electrode. Overpotentials were monitored with respect to a platinum counter electrode, and using an Ag/AgCl double-junction reference electrode. All electrodes were immersed in a jacketed glass electrochemistry cell containing ~50 ml of de-oxygenated sample solution. The temperature of the solution was controlled by pumping water through the cell jacket from an external temperature-controlled water bath. The equilibrium (or standard) potential (E^0) of sample solutions in the electrochemical cell were experimentally determined using cyclic voltammetry with variable sweep rates (Table S1, Fig. S1, Supplementary material). Applied overpotentials at which electrodeposition of metal occurred are calculated with respect to the experimentally determined E^0 values ($\eta = E - E^0$, Volts).

A series of electrodeposition experiments were performed as a function of applied overpotential, electrode rotation rate, and temperature. During each electroplating experiment, the applied potential was held constant for the amount of time required to deliver one Coulomb of charge (1 mol Zn = 2 × 96,485 C). Fresh 50 ml aliquots were taken from a batch stock solution and monitored to ensure that the isotopic and chemical composition of the reservoir remained unchanged (Supplementary Table S3). Representative plots of cell current as a function of applied overpotential, rotation rate, and temperature are shown in Figs. S1–S3of the Supplementary material. Additional experimental details are summarized in Table 1.

The electroplated zinc samples were removed and dissolved in warm 2% (w/v) HNO_3 in Teflon cups. The samples were evaporated to dryness and diluted with 4 ml of 2% HNO_3 and further diluted to a final concentration of 5 ppm for isotope analysis. The Zn concentration in dilutions was measured to estimate the total amount of metal electroplated (in moles). The ratio of this value to the total amount of charge passed in each experiment divided by Faraday's number (96,485 C/mol) × 2 (# electrons to reduce Zn^{+2} to Zn^0) provides a lower bound estimate of the efficiency of the plating reaction (Table 1) in competition with evolution of H_2 at the electrode. These efficiencies range from approximately 40–80%, with a general trend showing an increase in deposition efficiency with rotation rate. All reported currents in tables, figures and the text have been calculated with respect to the deposition efficiency (Table 1). Therefore, the rates reported are for the metal deposition reaction alone, not for the total current flowing throughout the three-electrode cell.

2.2. Isotope analysis

Isotope abundance analyses were performed using a Thermo-Finnigan Neptune Multi-collector Inductively Coupled Plasma Mass Spectrometer at the California Institute of Technology. Samples were introduced via a cyclonic spray chamber using an 80 µl/min PFA nebulizer. All samples and standards were diluted to a Zn concentration of 5 ppm and spiked with 5 ppm of an in-house Cu standard prior to analysis, at signal intensities of roughly 5 V ppm^{-1} for ^{63}Cu and 3 V ppm^{-1} for ^{64}Zn. Zinc samples were run alternately with a NIST SRM 682 standard, also spiked with Cu, which has previously been compared to JMC 3-0749L Zn (John et al., 2007). Signal intensity on ^{60}Ni, ^{63}Cu, ^{64}Zn, ^{65}Cu, ^{66}Zn and ^{68}Zn were monitored on cups L3, L2, L1, C, H1, and H2, respectively. Samples and standards were run alternately for three minutes each, with a 3 min rinse in between. The intensity of ^{60}Ni was used to correct for an interference of ^{64}Ni on ^{64}Zn, after estimating instrumental mass bias from the Cu isotope ratio, though ^{64}Ni corrections were always insignificant. Monitoring Cu isotope ratios in all samples and standards demonstrated that, within analytical error, there was no significant difference in mass bias for samples compared to standards, indicating that matrix effects were not important. All samples were therefore corrected for instrumental mass bias using only sample-standard bracketing, without a Cu-based mass bias correction. Each sample was measured at least three times, with the exception of sample Zn21 (Table 1). Table 1 summarizes the isotopic composition of samples relative to stock solutions and Table S3 (Supplementary material)presents the detailed three-isotope compositions of samples of electroplated zinc metal and stock solutions.

Observed fractionations are reported following the convention in which the ratio of the heavy stable isotope of zinc (^{H}Zn: H = 66 or 68) to the lightest stable isotope (^{64}Zn) is compared in per-mil (‰) deviation from a standard:

$$\delta^{H/64}Zn_{Sample} = 1000\left(\frac{(^{H}Zn/^{64}Zn)_{Sample}}{(^{H}Zn/^{64}Zn)_{Standard}} - 1\right) \quad (1)$$

In Table 1 and in most figures we report the observed isotope fractionation in electroplated Zn metal with reference to our measured average fractionation of the aqueous starting material as:

$$\Delta^{H/64}Zn_{metal-aqueous} = \delta^{H/64}Zn_{deposited\ metal} - \delta^{H/64}Zn_{aqueous\ solution} \quad (2)$$

Thus negative values of $\Delta^{H/64}Zn_{metal\text{-}aqueous}$ indicate that the plated metal is isotopically light in comparison with the stock solution.

Table 1
Summary of electrochemical experiments and MC-ICP-MS results.

	Temp (°C)	η (V)[a]	Rotation Rate (rpm)	Efficiency (%)[b]	Average current (mA/cm^2)	Levich current (mA/cm^2)	Δ^{66}Zn (‰) $\pm 2\sigma$[c]
Zn01	0	−0.2	2500	58.42	7.66	80.57	−3.62 ± 0.05
Zn02	0	−0.2	7500	59.35	8.03	139.55	−3.91 ± 0.05
Zn03	0	−0.3	2500	65.92	14.22	80.57	−2.57 ± 0.06
Zn04	0	−0.3	7500	67.43	16.22	139.55	−3.01 ± 0.05
Zn05	0	−0.5	1000	40.28	14.11	50.96	−2.23 ± 0.06
Zn06	0	−0.5	5000	49.71	20.15	113.94	−2.50 ± 0.05
Zn07	0	−0.5	7500	57.4	24.17	139.55	−2.65 ± 0.06
Zn08	0	−0.5	10,000	54.05	24.12	161.14	−2.74 ± 0.06
Zn09	25	−0.06	2500	79.23	2.55	157.17	−3.70 ± 0.06
Zn10	25	−0.1	2500	52.33	10.4	157.17	−3.59 ± 0.05
Zn11	25	−0.1	7500	50.63	10.53	272.22	−3.89 ± 0.06
Zn12	25	−0.2	2500	71.13	26.83	157.17	−2.85 ± 0.05
Zn13	25	−0.2	7500	71.07	29.75	272.22	−3.41 ± 0.05
Zn14	25	−0.3	2500	70.82	39.29	157.17	−1.97 ± 0.05
Zn15	25	−0.3	7500	77.95	50.13	272.22	−2.60 ± 0.05
Zn16	25	−0.5	1000	44.89	33.96	99.4	−1.56 ± 0.05
Zn17	25	−0.5	5000	61.27	59.37	222.27	−1.86 ± 0.07
Zn18	25	−0.5	7500	72.16	73.98	272.22	−2.01 ± 0.06
Zn19	25	−0.5	10,000	78.52	84.15	314.33	−2.08 ± 0.06
Zn20	25	−1	1000	31.25	55.95	99.4	−1.23 ± 0.06
Zn21	25	−1	5000	36.21	89.86	222.27	−1.31
Zn22	25	−1	7500	42.17	108.48	272.22	−1.45 ± 0.06
Zn23	25	−1	10,000	48.34	129.04	314.33	−1.49 ± 0.06
Zn24	50	−0.2	2500	66.02	56.26	267.78	−1.94 ± 0.06
Zn25	50	−0.2	7500	72.87	74.17	463.81	−2.62 ± 0.07
Zn26	50	−0.3	2500	78.67	86.95	267.78	−1.38 ± 0.06
Zn27	50	−0.3	7500	87.11	120.82	463.81	−2.06 ± 0.06
Zn28	50	−0.5	1000	54.41	70.62	169.36	−1.04 ± 0.06
Zn29	50	−0.5	5000	69.97	123.73	378.7	−1.31 ± 0.05
Zn30	50	−0.5	7500	75.61	148.56	463.81	−1.41 ± 0.06
Zn31	50	−0.5	10,000	81.58	167.26	535.57	−1.47 ± 0.05

[a] Overpotential, η, ($E - E^0$) relative to measured E^0 from CV spectra (Table S1).
[b] Percentage yield of metal plated (measured using AAS or ICP-MS) relative to the theoretical mass expected from charge delivered (see Section 2.1.).
[c] The isotopic composition of the samples is expressed as a per-mil deviation from the stock solution: $\Delta^{66}Zn = \delta^{66}Zn_{sample} - \delta^{66}Zn_{stock}$, where $\delta^{66}Zn = [(^{66}Zn/^{64}Zn)_{Sample}/(^{66}Zn/^{64}Zn)_{NIST} - 1] * 1000$; average value for three analyses. 2σ standard errors are reported. In all experiments, 1 coulomb of total charge was delivered.

3. RESULTS

Our experiments show that in all cases light isotopes of zinc are preferentially electroplated (Table 1), with observed fractionations ranging from −1.04(6)‰ to −3.91(5)‰. Fig. 1a shows the mass dependent nature of the isotope fractionation on a three isotope plot. Fig. 1b shows deviations from a calculated mass-dependence law governing equilibrium fractionation processes following the relationships calculated using formalism described by Young et al. (2002). This plot shows that as a whole, our data follows the slope of a kinetic fractionation law and is clearly resolvable from an equilibrium law. The values on Fig. 1b all lie below the zero line because of the small non-zero intercept of the measured three isotope data arising from the isotopic composition of the starting solution.

A summary of results of the electroplating experiments (Fig. 2) shows that observed isotope fractionation has strong systematic dependencies on overpotential, temperature, and electrode rotation rates with larger fractionations occurring at low overpotentials, low temperatures, and fast rotation rates. Fig. 3 shows fractionation as a function of rotation rate and overpotential at 25 °C, showing that fractionation tends to increase as stir rate increases. Also shown on this plot are results from deposition studies on planar glassy carbon electrodes, which are performed without hydrodynamic mass-transport. These results also emphasize different fractionations observed using different starting solutions (Black et al., 2010a). The open circles represent the same citrate-based solution chemistry as used in this RDE study, and the observed fractionation factors are consistent in magnitude but differ in spread over a range of overpotentials. Generally the observed fractionations in these experiments using Zn-citrate solutions are smaller than the fractionation factors observed in metal deposited from acidified sulfate solutions.

Fig. 4 shows measured isotope fractionation as a function of temperature compared with calculated temperature-dependent equilibrium fractionations between Zn metal and Zn citrate complex (Black et al., 2011b). The

measured temperature dependence is generally steeper than the predicted equilibrium-temperature dependence. A comparison between calculated equilibrium fractionations and observed fractionations are also shown in Fig. 2. At low overpotentials, closer to equilibrium potential of the electrochemical process, the measured fractionations are larger than the predictions of equilibrium fractionation. At the largest overpotentials, the measured fractionation is less than the calculated equilibrium values. Previous experiments exhibited larger fractionations in deposited Zn metal (squares and triangles plotted at a rotation rate of 0 in Fig. 3, Black et al., 2010a), which we attribute to differences in the starting solution chemistry – the larger fractionations are observed especially in acidified solutions – and therefore to differences in the reactive species at the electrode surface.

The observed negative correlation between temperature and isotopic fractionation in these experiments contrasts with our earlier study (Black et al., 2010a), which showed that zinc isotope fractionation during plating on a planar electrode increases as temperature increases (Fig. 4). To help interpret the reversal of the temperature trend in the two sets of experiments, we describe a simple forward model that provides a qualitative explanation for this apparent reversal based on the competition of two kinetic mechanisms with very different activation energies. Our forward model is described in the next section.

4. DEPOSITION RATES AND MASS-TRANSPORT AT A ROTATING DISC ELECTRODE

The Levich equation describes the observed current for an electrochemical reaction at a rotating disc electrode, where rates are limited by convective-diffusive mass transport (Bard and Faulkner, 2001), and is given by:

$$i_l = 0.62nFAC_0^* D^{2/3}\omega^{1/2}v^{-1/6} \quad (3)$$

where i_l is the Levich current (mass-transport-limited), n is the number of electrons transferred in the reaction, F is Faraday's constant, C_0^* is the bulk concentration in solution, D is the diffusion coefficient, ω is the angular rotation rate, and v is the kinematic viscosity of the solution. Note that both the diffusion coefficient and the kinematic viscosity are dependent on temperature, so the Levich equation will also have a temperature dependence. To extrapolate the diffusion coefficient at infinite dilution (Vanysek, 2007–2008) to higher and lower temperatures, an Arrhenius relationship ($D_M = D_M^0 \exp(-E_A/RT)$) is used, where D_M^0 and E_A are the experimentally-determined pre-exponential factor and activation energies, R is the gas constant, and T is the temperature. We used the temperature-dependent kinematic viscosity given by Kestin et al. (1978). Calculated values for the Levich current are shown in Table 1.

The kinetic behavior of our electroplating experiments is accurately described by this relationship, as demonstrated on a Levich plot (Fig. 5) which shows a linear relationship between the measured current as a function of the square root of rotation rate. The slopes are temperature dependent, arising from the temperature dependence of both the diffusion coefficient and kinematic viscosity terms. If the overall reaction current were controlled solely by the mass transport step, then the y-intercepts on Fig. 5 would fall on zero. The fact that they do not indicates that the kinetics are controlled by at least a second governing process.

Additional support for this dual-control hypothesis is provided by a plot of fractionation as a function of dimensionless current where the observed current is normalized to the calculated Levich current for each experiment (Fig. 6). To calculate the Levich current for each experiment, we use experimentally-determined measurements of the diffusivity of Zn^{+2} in solution and an experimentally measured activation energy (~22.1 kJ mol^{-1}) to calculate

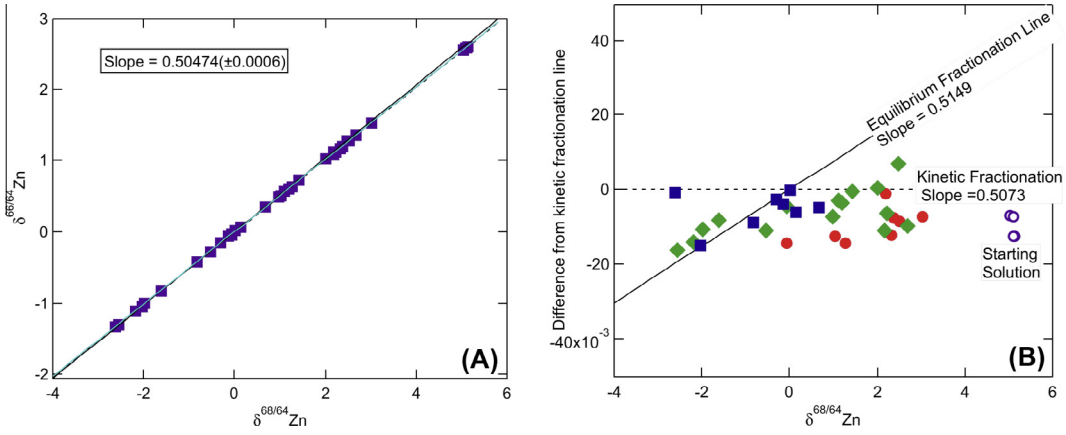

Fig. 1. (A) Three isotope plot showing all of the measured Zn isotope data with respect to the NIST standard. The solid black line shows a calculated fractionation with respect to the starting solution ($\delta^{66}Zn = 2.58$, $\delta^{68}Zn = 5.1$) according to equilibrium processes. Measurement errors are shown in Table 1, but not on the plot for clarity in seeing trend. The dashed line shows a calculated fractionation according to a kinetic fractionation law (Young et al., 2002). (B) Deviation from a predicted kinetic mass-dependent slope (dashed line) using formalism from Young et al. (2002). The predicted equilibrium fractionation is shown as a solid black line. Blue square, green diamond, and red circle symbols correspond to experiments at 0, 25, and 50 °C. (For interpretation of the references to colour in this figure legend, the reader is referred to the web version of this article.)

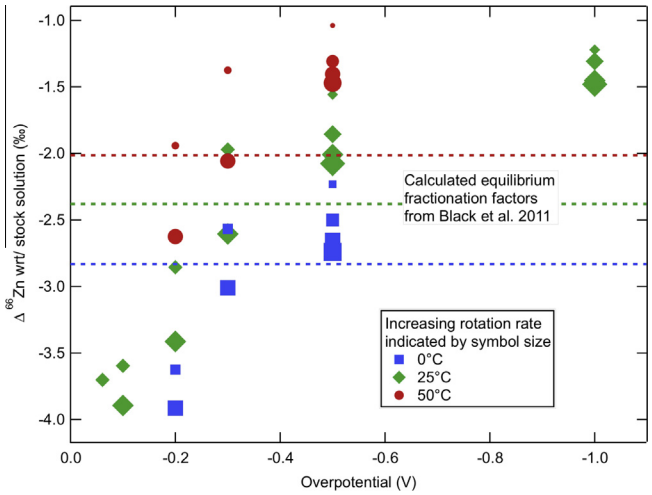

Fig. 2. Measured $\Delta^{66/64}$Zn of metallic zinc, with respect to the stock solution, as a function of overpotential, rotation rate (increasing symbol size with increasing rotation rate from 1000 to 10,000 rpm), and temperature. Horizontal dashed lines show calculated equilibrium fractionation factors from Black et al., 2011b.

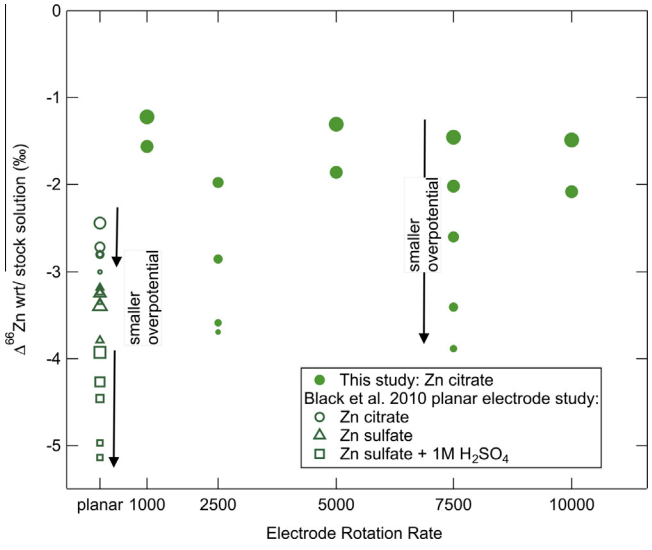

Fig. 3. Isotope fractionation as a function of electrode rotation rate at 25 °C. The symbol size decreases with decreasing overpotential, as emphasized by arrows. Results from the planar electrode study of Black et al., 2010a are shown as open symbols. Open circles are planar electrodeposition experiments using the same citrate buffered chemistry as used in this study. Triangles are from a $ZnSO_4$ starting solution, with no pH buffer. Squares are from an acidified $ZnSO_4$ starting solution.

its temperature dependence (Adhyapak, 1986). In calculating the Levich current, we use values for the temperature-dependent kinematic viscosity of water, equal to 1.793 mm^2/s at 0 °C, 0.8928 mm^2/s at 25 °C, and 0.553 mm^2/s at 50 °C (Kestin et al., 1978).

The measured Zn isotope fractionation falls along a log-linear trend when plotted as a function of dimensionless current (Fig. 6), the measured current normalized by the transport-limited current and this trend occurs over several orders of magnitude in the deposition rate. If mass-transport limitations played no role in the isotope behavior, and fractionation was only due to a chemical reaction, the observed fractionation would be constant on this plot. If only the mass transport effect contributed an isotope fractionation, then this plot would show zero fractionation at low current, increasing to larger fractionations at the highest currents. Our observation of large fractionations at low currents decreasing to smaller fractionations at high currents demonstrates that (at least) two independent processes are responsible for the overall isotope fractionation kinetics. This result is similar to our previous observations for room-temperature iron deposition experiments using a rotating disc electrode (Black et al., 2010b).

To investigate how temperature-dependent processes may affect the isotope fractionations in an electroplating experiment we build a forward model describing the isotope

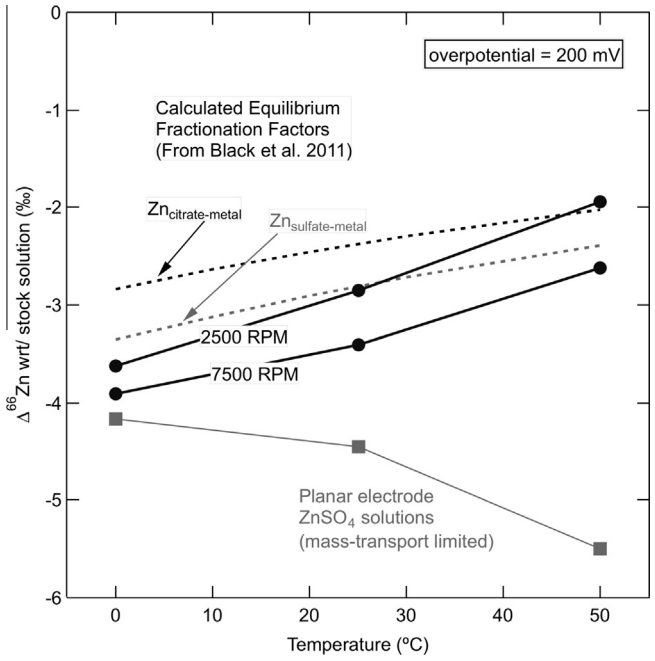

Fig. 4. Fractionation at constant overpotential as a function of temperature at two different electrode rotation rates. The black circles show measured Zn isotope fractionation as a function of temperature at slow and fast rotation rates and 200 mV overpotential. Gray squares and lie show observed fractionations as a function of temperature for electrodeposition on planar electrodes from $ZnSO_4$ solutions (Black et al., 2010a). Dashed lines show calculated temperature-dependent equilibrium fractionation factors between Zn metal and Zn citrate (black) and Zn metal and bidentate inner-sphere Zn sulfate (gray) from Black et al. (2011b).

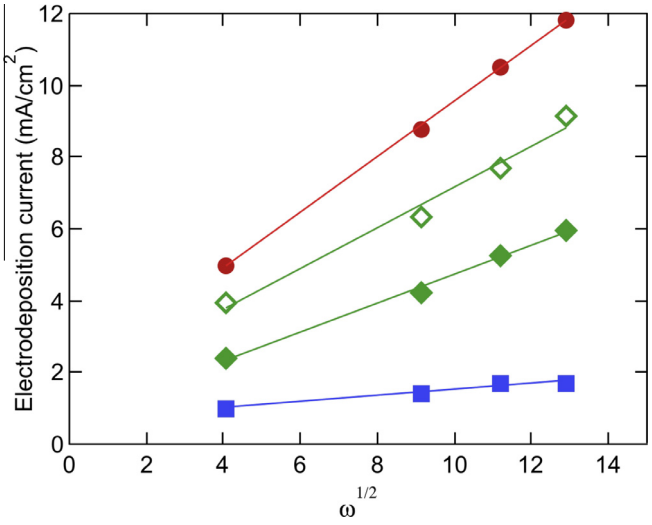

Fig. 5. Levich plot of current as a function of the square root of rotation rate (Eq. (3)) during the Zn electroplating experiments. Closed symbols: −500 mV; open symbols −1000 mV. Red circles: 50 °C, green triangles: 25 °C, blue squares 0 °C. (For interpretation of the references to color in this figure legend, the reader is referred to the web version of this article.)

kinetics of an electroplating process under two competing kinetic controls, an electrochemical step and a mass-transport limited step. The model is based on the Koutecky–Levich equation (Koutecky and Levich, 1958), which describes the overall rate of a chemical reaction under simultaneous control of mass-transport-limited processes (i_{Levich}) and electrochemical processes ($i_{\text{electrode}}$), and is given by:

$$\frac{1}{i_{\text{total}}} = \frac{1}{i_{\text{Levich}}} + \frac{1}{i_{\text{electrode}}} \tag{4}$$

where i_{Levich} is the rate (current) corresponding to a mass transport process, given by Eq. (3) and $i_{\text{electrode}}$ is the rate of an electrochemical process at an electrode, and is given by the Butler–Volmer equation $i_{\text{electrode}} = k^0 \exp(\kappa n F \eta / RT)$, where k^0 is a pre-exponential factor, κ

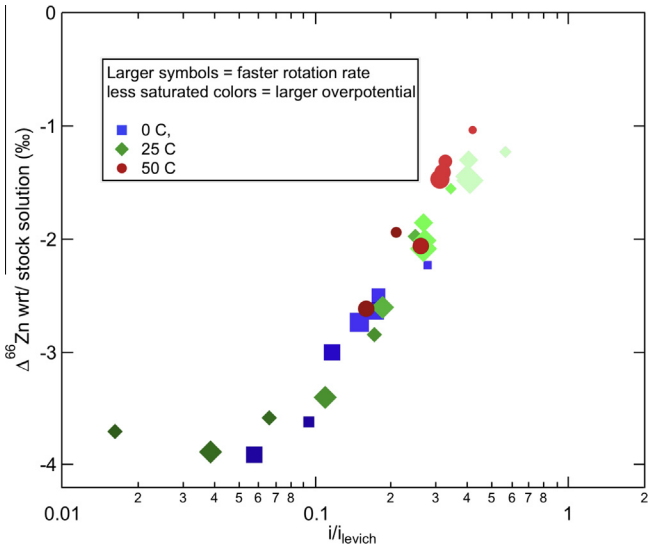

Fig. 6. Fractionation as a function of average measured current normalized to the calculated Levich (transport rate-limiting) current.

is a reaction symmetry factor, n is the number of electrons transferred in the reaction which is equal to 2 in this case of Zn reduction, F is Faraday's constant equal to 96,485 C/mol, η is the overpotential, R is the ideal gas constat and T is the temperature in K. The form of the Butler–Volmer equation is an approximation is only valid far from equilibrium, which is an appropriate description of our experiments. The mass-dependent behavior of such a reaction was derived in a recent study (Black et al., 2010b), and the fractionation is given by the ratio of the rates (currents) for the heavy isotope and the light isotope, as given by:

$$\frac{{}^{H}i_{observed}}{{}^{L}i_{observed}} = \frac{1}{\frac{{}^{L}i_{electrode}}{{}^{H}i_{electrode}} + \frac{{}^{L}i_{electrode}}{{}^{H}i_{Levich}}} + \frac{1}{\frac{{}^{L}i_{Levich}}{{}^{H}i_{Levich}} + \frac{{}^{L}i_{Levich}}{{}^{H}i_{electrode}}} \quad (5)$$

where Eqs. (6)–(8)describe the ratios in the denominators of Eq. (5) as follows:

$$\frac{L_{i_{electrode}}}{H_{i_{electrode}}} = \frac{{}^{L}k^{0}}{{}^{H}k^{0}} e^{({}^{H}\kappa - {}^{L}\kappa)nF\eta/RT} \quad (6)$$

$$\frac{{}^{L}i_{Levich}}{{}^{H}i_{Levich}} = \frac{{}^{L}D_{M}^{2/3}}{{}^{H}D_{M}^{2/3}} \left(\frac{0.893 + 0.316({}^{H}D_{M}/v)^{0.36}}{0.893 + 0.316({}^{L}D_{M}/v)^{0.36}} \right) \quad (7)$$

$$\frac{{}^{L}i_{electrode}}{{}^{H}i_{Levich}} \approx \frac{{}^{H}i_{Eeectrode}}{{}^{L}i_{Levich}} = \frac{k^{0} e^{-\kappa nF\eta/RT} \left(0.893 + 0.316(D_{M}/v)^{0.36}\right)}{0.554 D_{M}^{2/3} v^{-1/6} \omega^{1/2}} \quad (8)$$

In Eq. (6), ${}^{L}k^{0}$ and ${}^{H}k^{0}$ are the pre-exponential rate factors for the light (L) and heavy (H) isotopes, respectively.

Eqs. (5)–(8)predicts isotope fractionation arising from a coupled electrochemical/mass-transport process, which can be broken down into an electrochemical term (Eq. (6)), a diffusive term (Eq. (7)) and the coupled electrochemical/mass-transport terms (Eq. (8)). To calculate the isotope-dependent Koutecky–Levich behavior, we use measurements of the isotope fractionation due to diffusion in aqueous systems for Zn as determined by Rodushkin et al. (2004), and viscosity measurements by Kestin et al. (1978). Forward models of the behavior of Eqs. (5)–(8)were performed in an earlier study and compared favorably with data on Fe isotope fractionation during electroplating (Black et al., 2010b). Our models show that our observed trends can be reproduced with a combination of diffusive, equilibrium and electrochemically driven fractionation, with larger fractionations being produced under electrochemical kinetic control (Fig. 7). However, in the earlier study, no conclusions could be made about the temperature-dependent behavior, because the experiments were only performed at room temperature (Black et al., 2010b).

Eqs. (5)–(8)contain several temperature-dependent variables, including electrochemical reaction rates, viscosity and diffusion. Both the electrodeposition reaction and mass transport kinetics can be cast in terms of thermally activated kinetic processes; and generally will have different activation energies. The temperature dependence of k^{0} is harder to define, as it is not explicit in Butler–Volmer theory. Extensions of charge transfer theory (Marcus, 1964, 1993) show that this pre-exponential factor is proportional to square root of temperature, however, make no predictions about whether the mass-dependence of the k^{0} parameter will also be temperature dependent. For the purposes of discussion here we will assume that the temperature dependence of the ratio ${}^{64}k^{0}/{}^{66}k^{0}$ is proportional to $1/T^{2}$, and the magnitude of this ratio scales with the predicted equilibrium fractionation between metallic and aqueous species (Black et al., 2011a). Whether or not other parameters, such as κ, are also temperature dependent is unknown. Therefore, we assume that κ is independent of temperature. Using these assumptions the temperature dependent predictions of Eqs. (5)–(8)can be evaluated quantitatively.

The primary observation that we need to explain is the increase in isotope fractionation with increasing temperature that we observe in the planar electrode data (Black et al., 2011a,b) and reverse trend that we observe in the RDE data (Fig. 4). Our model provides a possible

explanation, as shown in Fig. 7. In order to interpret the data we must consider not only the relative rates of the diffusion process and electrochemical reaction, but also their relative temperature dependencies. The parameter space of these two governing behaviors is mapped out in Fig. 7, which qualitatively models the rate and fractionation behavior for several different combinations of the absolute values and temperature dependencies of the rates of these two processes. The top row shows schematics of diffusion rates with a given activation energy E_D (black lines). In each plot, four different values of the diffusion rate are shown, with the same activation energy, but representing cases that have slow mass transport and fast mass transport. The green line in Fig. 7 demonstrates three cases for the relative activation energy of the electrochemical reaction step E_R which may be greater than (left), equal to (middle) or less than (right) that for the diffusion step. The bottom row of figures shows a series of curves of calculated isotope fractionations for all of the cases. The case at the right qualitatively duplicates our main experimental observation, in which we observe fractionations increasing with temperature for low diffusion rates, such as at a planar electrode, and fractionation decreasing with temperature for high diffusion rates, such as at a rotating disc electrode. However, we only see this case when the effective activation energy for the electrode transfer is lower than that for the diffusion process.

The models results plotted Fig. 7 are meant to provide a qualitative assessment of how competition between two rate-determining steps can generate very different overall observed fractionations and temperature dependences, depending on the overall rate. We use our model and Eq. (8)to provide a forward prediction of isotope fractionation during Zn electroplating as a function of temperature, rotation rate, and overpotential (Fig. 8).

A quantitative examination of the predicted fractionation during electroplating as modeled by Eq. (8)is shown in Fig. 8, which plots the predicted isotope fractionation as a function of temperature (Fig. 8A), RDE rotation rate (Fig. 8B) and applied overpotential (Fig. 8C). Fig. 8 shows that at low overpotentials and high rotation rates, isotope fractionation increases with decreasing temperature, consistent with equilibrium stable isotope theory (Bigeleisen and Mayer, 1947; Urey, 1947) and our observations shown in Fig. 4. Fig. 8 also demonstrates how with increasing overpotential and decreasing rotation rate, the temperature trends can reverse and the opposite trend may be observed, due to competition between electrochemical kinetics and mass transport kinetics. We observe this temperature-trend reversal in our deposition experiments of Zn on a planar electrode (Black et al., 2010a), as shown by the gray squares in Fig. 4.

The take-home message from our models and experiments is that when two (or more) competing kinetic processes control the overall rate of a process such as a redox process or precipitation process, the observed fractionation factors can vary as a function of rate or temperature in ways that may appear non-intuitive at first, such as an increase of observed fractionation with increasing temperature at high rates changing to an opposite temperature

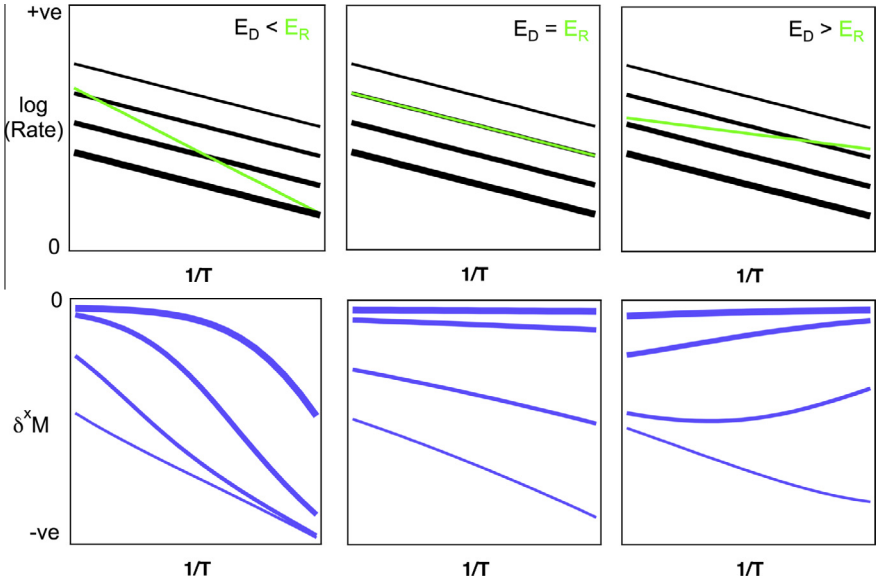

Fig. 7. Model calculations showing the temperature dependence of competing rates (top three plots) and corresponding isotope fractionation (bottom three plots). In the top plots, the black lines correspond to a diffusion process with a constant activation energy, but with variations in the absolute value of the diffusion coefficient leading to different absolute rates. The green lines show rates of an electrochemical process that has a lower (left), equal (middle), and larger (right) activation energy than the diffusion process. The three plots below show calculated isotope fractionation as a function of inverse temperature for the three cases above, and as a function the four overall mass transport rate. The case at the right demonstrates that the temperature dependence of isotope fractionation shifts from positive correlation at low diffusion rates to negative correlation at high diffusion rates. The relative isotope fractionation is calculated for a fixed $\delta^x Mreact/\delta^x Mdiff = 50$ (e.g. $\delta^{66/64}Zn_{diff} = -0.1‰$ and $\delta^{66/64}Zn_{react} = -5‰$). (For interpretation of the references to colour in this figure legend, the reader is referred to the web version of this article.)

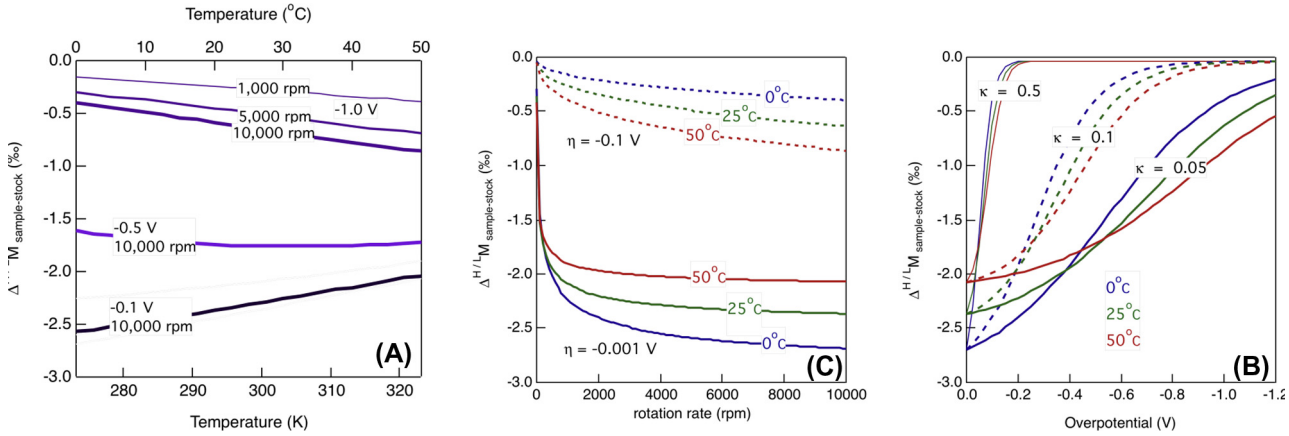

Fig. 8. Forward model of the mass-dependent Koutecky–Levich equation (Eq. (8)) showing the effect of temperature on predicted fractionation. At high rotation rates and low overpotentials the fractionation decreases with increasing temperature, but at low rotation rates and high overpotentials, the fractionation is predicted to increase with increasing temperature. (A) $\Delta^{H/L}M$ vs. temperature, $\kappa = 0.05$; (B) $\Delta^{H/L}M$ vs. RDE rotation rate, $\kappa = 0.5$; (C) $\Delta^{H/L}M$ vs. applied overpotential, $\omega = 10{,}000$ rpm. $k^0 = 1E\text{-}5$. Calculations were performed using diffusion coefficients for Zn and ${}^{L}D/{}^{H}D = 1.000058$. ${}^{L}k^0/{}^{H}k^0 = 1.00298$ (at 0 °C), 1.00253 (at 25 °C) and 1.00217 (at 50 °C) (following a fractionation $\propto 1/T$ relationship) to reflect changes in predicted equilibrium fractionation.

trend at low rates. Our forward models show, however, that overall observed fractionations arising from competing kinetic processes are predictable.

5. CONCLUSIONS

The fractionation of zinc stable isotopes during the electrodeposition of $Zn_{(s)}$ from Zn citrate solutions is large, producing fractionations on the order of $-1‰$ to $-3.9‰$ in $\delta^{66/64}Zn$. These fractionation values are larger than predicted equilibrium fractionation factors, and larger than the isotope signatures observed in nature (ref). Collectively, the data appear to follow a kinetic mass-dependent fractionation law when plotted in three-isotope space. However, at a constant temperature, the three-isotope slope is intermediate between an equilibrium and a kinetic mass-fractionation law.

The use of a rotating disc electrode helps control mass-transport conditions within an electrochemical cell and allows for an evaluation of the kinetic regime controlling isotope fractionation during electroplating. At slow rotation rates and large overpotentials, the electroplating kinetics of are limited by mass transport of the species to an electrode. In this case, increasing the temperature increases the mass transport rate more than the deposition rate, causing an increase in observed fractionation with increased temperature. When the mass transport limitations are reduced using a fast electrode rotation rate and low overpotentials, the temperature dependence is similar to that predicted by equilibrium stable isotope fractionation theory (Black et al., 2011b). This reversal of temperature-dependent behavior is predicted by the models and observed in the experiments.

Most electrochemical processes occur at overall rates arising from at least two major intertwined processes: mass transport at the electrode, and the electrode rate-limiting step. It is almost impossible to imagine a single rate-limiting process that can explain all of the data, especially the reversing of sense of the temperature dependent fractionation between the planar electrode experiments and the rotating disc electrode experiments. We can explain the qualitative behavior of both the observed currents and the observed fractionations in both the planar electrode and the rotating disc electrode with two competing rates; however the requirements on the relevant parameters are stringent – namely, the activation energy of the diffusion (or mass transport) process must be higher than the chemical electrodeposition effective activation energy, while the absolute values of the two rates must be approximately the same. Given these two criteria, it is surprising to us that we see similar qualitative behavior in our studies of isotope electroplating in Fe (Kavner et al. 2009; Black et al., 2010a,b), Li (Black et al., 2009), and Cu (Black et al., 2011a). Isotope behavior observed during processes that couple these competing reaction rates provide an additional window to examine the behavior of the rates of multistep chemical reactions.

ACKNOWLEDGMENTS

We thank Professor Edwin Schauble for his input and discussion of equilibrium isotope effects and Professor Jess Adkins for access to facilities at Caltech. We thank Jeffrey Crawford for assistance with the Zn electroplating experiments. This work was funded by the US Department of Energy: Division of Chemical Sciences, Geosciences, & Biosciences DE-FG02-10ER16136 (A.K.).

APPENDIX A. SUPPLEMENTARY DATA

Supplementary data associated with this article can be found, in the online version, at http://dx.doi.org/10.1016/j.gca.2013.09.016.

REFERENCES

Adhyapak N. G. (1986) Activation energy of self-diffusion of zinc, chloride and chromate ions. *J. Radioanal. Nucl. Chem.* **103**, 379–385.

Arnold T., Kirk G. J. D., Wissuwa M., Frei M., Zhao F.-J., Mason T. F. D. and Weiss D. J. (2010) Evidence for the mechanisms of zinc uptake by rice using isotope fractionation. *Plant, Cell Environ.* **33**, 370–381.

Bard A. J. and Faulkner L. R. (2001) *Electrochemical METHODS: Fundamentals and Applications*. John Wiley & Sons Inc., USA.

Bigalke M., Weyer S., Kobza J. and Wilcke W. (2010) Stable Cu and Zn isotope ratios as tracers of sources and transport of Cu and Zn in contaminated soil. *Geochim. Cosmochim. Acta* **74**, 6801–6813.

Bigeleisen J. and Mayer M. G. (1947) Calculation of equilibrium constants for isotopic exchange reactions. *J. Chem. Phys.* **15**, 261–267.

Black J. R., Umeda G., Dunn B., McDonough W. F. and Kavner A. (2009) The electrochemical isotope effect and lithium isotope separation. *J. Am. Chem. Soc.* **131**, 9904–9905.

Black J. R., John S., Young E. D. and Kavner A. (2010a) Effect of temperature and mass-transport on transition metal isotope fractionation during electroplating. *Geochim. Cosmochim. Acta* **74**, 5187–5201.

Black J. R., Young E. and Kavner A. (2010b) Electrochemically controlled iron isotope fractionation. *Geochim. Cosmochim. Acta* **74**, 809–817.

Black J. R., Crawford J. J., John S. and Kavner A. (2011a) Redox-driven stable isotope fractionation, Tratnyek, P. G. , Grundl, T. J. and Haderlein, S. B. (eds.). *Aquatic Redox Chemistry*. *ACS Symposium Series* **1071**, 345–359 (Chapter 16).

Black J. R., Kavner A. and Schauble E. A. (2011b) Calculation of equilibrium stable isotope partition function ratios for aqueous zinc complexes and metallic zinc. *Geochim. Cosmochim. Acta* **75**, 769–783.

Borrok D. M., Wanty R. B., Ridley W. I., Lamothe P. J., Kimball B. A., Verplanck P. L. and Runkel R. L. (2009) Application of iron and zinc isotopes to track the sources and mechanisms of metal loading in a mountain watershed. *Appl. Geochem.* **24**, 1270–1277.

Chen J., Gaillardet J., Louvat P. and Huon S. (2009) Zn isotopes in the suspended load of the Seine River, France: Isotopic variations and source determination. *Geochim. Cosmochim. Acta* **73**, 4060–4076.

Cloquet C., Carignan J., Lehmann M. F. and Vanhaecke F. (2008) Variation in the isotopic composition of zinc in the natural environment and the use of zinc isotopes in biogeosciences: A review. *Anal. Bioanal. Chem.* **390**, 451–463. http://dx.doi.org/10.1007/s00216-007-1635-y.

Fernandez A. and Borrok D. M. (2009) Fractionation of Cu, Fe, and Zn isotopes during the oxidative weathering of sulfide-rich rocks. *Chem. Geol.* **264**, 1–12.

Fujii T. and Albarède F. (2012) Ab initio calculation of the Zn isotope effect in phosphates, citrates, and malates and applications to plants and soil. *PLoS One* **7**(2), e30726.

Fujii T., Moynier F., Pons M. L. and Albarede F. (2011) The origin of Zn isotope fractionation in sulfides. *Geochim. Cosmochim. Acta* **75**, 7632–7643. http://dx.doi.org/10.1016/j.gca.2011.09.036.

Gagnevin D., Boyce A. J., Barrie C. D., Menuge J. F. and Blakeman R. J. (2012) Zn, Fe and S isotope fractionation in a large hydrothermal system. *Geochim. Cosmochim. Acta*, 183–198. http://dx.doi.org/10.1016/j.gca.2012.04.031.

John S. G., Park J. G., Zhang Z. and Boyle E. A. (2007) The isotopic composition of some common forms of anthropogenic zinc. *Chem. Geol.* **245**, 61–69.

Jouvin D., Weiss D. J., Mason T. F. M., Bravin M. N., Louvat P., Zhao F., Ferec F., Hinsinger P. and Benedetti M. F. (2012) Stable isotopes of Cu and Zn in higher plants: Evidence for Cu reduction at the root surface and two conceptual models for isotopic fractionation processes. *Environ. Sci. Technol.* **46**, 2652–2660.

Juillot F., Marechal C., Morin G., Jouvin D., Cacaly S., Telouk P., Benedetti M. F., Ildefonse P., Sutton S., Guyot F. and Brown, , G. E. (2011) Contrasting isotopic signatures between anthropogenic and geogenic Zn and evidence for post-depositional fractionation processes in smelter-impacted soils from Northern France. *Geochim. Cosmochim. Acta* **75**, 2295–2308.

Kavner A., Bonet F., Shahar A., Simon J. and Young E. (2005) The isotopic effects of electron transfer: An explanation for Fe isotope fractionation in nature. *Geochim. Cosmochim. Acta* **69**, 2971–2979.

Kavner A., John S. G., Sass S. and Boyle E. A. (2008) Redox-driven stable isotope fractionation in transition metals: Application to Zn electroplating. *Geochim. Cosmochim. Acta* **72**, 1731–1741.

Kavner A., Shahar A., Black J. R. and Young E. (2009) Iron isotopes at an electrode: Diffusion-limited fractionation. *Chem. Geol.* **267**, 131–138.

Kestin J., Sokolov M. and Wakeham W. A. (1978) Viscosity of liquid water in the range −8 °C to 150 °C. *J. Phys. Chem. Def. Data* **7**(#3), 941–948.

Koutecky J. and Levich V. G. (1958) The use of a rotating disk electrode in the study of electrochemical kinetics and electrolytic processes. *Zh. Fiz. Khim.* **32**, 1565–1575.

Marcus R. A. (1964) Generalization of the activated complex theory of reaction rates. I. Quantum mechanical treatment. *J. Chem. Phys.* **41**, 2614–2623.

Marcus R. A. (1993) Electron-transfer reactions in chemistry: Theory and experiment (Nobel lecture). *Angew. Chem.* **105**, 1161–1172.

Mattiellia N., Petit J., Deboudt K., Flament P., Perdrix E., Taillez A., Rimetz-Planchon J. and Weis D. (2009) Zn isotope study of atmospheric emissions and dry depositions within a 5 km radius of a Pb–Zn refinery. *Atmos. Environ.* **43**, 1265–1272.

Moynier F., Pichat S., Pons M. L., Fike D., Balter V. and Albarede F. (2009) Isotopic fractionation and transport mechanisms of Zn in plants. *Chem. Geol.* **267**, 125–130.

Rodushkin I., Stenberg A., Andren H., Malinovsky D. and Baxter D. C. (2004) Isotopic fractionation during diffusion of transition metal ions in solution. *Anal. Chem.* **76**, 2148–2151.

Toutain J. P., Sonke J., Munoz M., Nonell A., Polvé M., Viers J., Freydier R., Sortino F., Joron J. L. and Sumarti S. (2008) Evidence for Zn isotopic fractionation at Merapi volcano. *Chem. Geol.* **253**, 74–82.

Urey H. C. (1947) Thermodynamic properties of isotopic substances. *J. Chem. Soc.*, 562–581.

Vanysek P. (2007–2008) Ionic conductivity and diffusion at infinite dilution. In *CRC Handbook of Chemistry and Physics* (ed. D. R. Lide).

Weiss D. J., Mason T. F. D., Zhao F. J., Kirk G. J. D., Coles B. J. and Horstwood M. S. A. (2005) Isotopic discrimination of zinc in higher plants. *New Phytol.* **165**, 703–710.

Young E. D., Galy A. and Nagahara H. (2002) Kinetic and equilibrium mass-dependent isotope fractionation laws in nature and their geochemical and cosmochemical significance. *Geochim. Cosmochim. Acta* **66**, 1095–1104.

Associate editor: Frederic Moynier